

A GENERIC SHELL MODEL FOR INSTRUMENTS OF THE VIOLIN FAMILY

CE Gough School of Physics and Astronomy, University of Birmingham, B15 2TT, UK.

1 INTRODUCTION

A number of simple models have been introduced to describe the low frequency vibrational modes of the violin, notably the Beldie mass-spring model described in mathematical detail by Cremer¹. The modes of the doubly-arched violin body have also been compared to those of a cylindrical shell, used in many textbooks as an introduction to flexural waves on curved surfaces (for example, Calladine²). However, none of these models adequately describe the strongly radiating *CBR*, *B1*- and *B1+* signature modes responsible for almost all the radiated sound of the violin below around 1 kHz, let alone the higher frequency modes.

In contrast, our knowledge of the vibrational modes of violins has advanced rapidly in recent years. This has largely been due to experimental modal analysis measurements pioneered by Marshall³ and in later extensive measurements by Bissinger⁴ and Stoppani⁵. Such measurements have provided detailed information about the vibrational modes and acoustic properties of many fine Stradivari, Guarneri and modern violins, as well as less valuable instruments. In addition, finite element computations, notably by Knott⁶, Roberts⁷, Rogers and Anderson⁸ and Bretos et al.⁹, have described many modes of the violin in terms of their underlying physical properties.

The present model is similarly based on a finite element approach, but aimed at understanding rather than simply reproducing the mode shapes and frequencies of a specific instrument. The model suggests that the dynamics of all instruments of the violin family can be described as the modes of a shallow, thin-walled, doubly arched, guitar-shaped, box-like shell structure. Surprisingly, there are very few published examples of the dynamical modes of even rectangular box shell structures, let alone shallow boxes with arched or shaped plates. In all such structures, the plates and ribs introduce strong boundary conditions around their edges resulting in a very different set of vibrational modes than those of a cylindrical shell.

By varying the geometric size, physical properties and coupling strengths over a wide range of values, the present model illustrates a direct relationship between the modes of the free top and back plates and those of the assembled instrument. The model shows how the flexural plate modes of the assembled shell, before adding the soundpost, *f*-holes, base bar, neck and fingerboard, form a set of component or basis modes. These modes are then coupled together by the soundpost and other structural components, to form the non-interacting normal modes of the instrument, observed as strong resonances in admittance and acoustic radiation measurements.

In addition to providing a coherent model, potentially describing the vibrational modes of all instruments of the violin family, it is hoped that the model will provide makers with some helpful insights into the way that the various component parts of the fully assembled body couple together, to give the characteristic acoustic properties of individual instruments.

2 FINITE ELEMENT MODE

The finite element geometry of the violin illustrated in Fig.1 is loosely based on the internal rib outline, arching and other physical dimensions of the Titian Strad (Zygmuntowicz¹⁰). As we are interested in the vibrational properties of all instruments of the violin family, the exact dimensions and detailed geometry are of secondary importance. Variations in physical and geometric properties

can always be included later as relatively small perturbations, changing specific mode frequencies, but not their underlying shapes. The model will be described in detail in a separate publication.

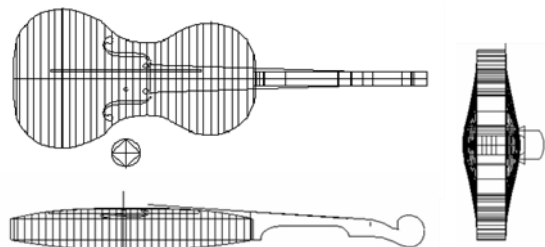


Figure . The unmeshed geometric model used for the finite element computations illustrating the guitar-shaped outline and arching of the plates and schematic representation of the neck. The transverse and longitudinal lines indicate the cross-sections along which the arching profiles were defined. The circular disc is used to demonstrate the induced f -hole Helmholtz vibrations.

The unmeshed geometric model used for the finite element computations is illustrated in figure 1. The 15 mm high arching profiles of the plates were defined by simple mathematical functions, with identical top and back plate profiles across the width, but slightly different profiles along the length.

For initial simplicity, plates of uniform thickness have initially been considered, with uniform elastic properties representing the geometric mean of the anisotropic properties along and across the grains. This ensures the correct mode density at high frequencies (Cremer¹, chpt.10). The plate thicknesses, densities and elastic constants were chosen to closely match typical front and back plate masses and free plate mode #2 and #5 frequencies. The influence on mode shapes and frequencies of elastic anisotropy and graduations of plate thicknesses will be described in a later paper.

An underlying assumption in taking the above approach is that the mode shapes and frequencies of the assembled instrument will largely depend on the modal frequencies and masses of the free plates rather than how such values are determined by the specific arching, elastic anisotropies and thickness graduations used to achieve them. This is a very similar approach to that taken by those makers who tune free plate frequencies and mode shapes before assembling the instrument.

To investigate the influence of the ribs, f -holes, bass bar, soundpost, neck and fingerboard on mode shapes and frequencies, their strengths have been varied from zero to typical normal values. In addition, the important influence of soundpost position both along and across the length of the instrument has been investigated. The influence of internal air resonances and the Helmholtz f -hole resonances in particular is also described.

The addition of corner and end blocks, linings, plate over-hangs, tailpiece, fingerboard and string resonances can all be incorporated into the model later, either as minor perturbation of factors like the effective rib mass and elastic strength or as weakly coupled resonators in the case of the fingerboard, tailpiece, strings and higher order cavity air resonances.

Although all the computations presented in this paper are for the violin, the mode shapes and dependencies of modal frequencies on physical and geometric factors are expected to be much the same for instruments of any size, as the symmetry of the modes is largely determined by the symmetry of the shell structure, which is much the same for all instruments of the violin family.

The computations were made using the structural mechanics shell module of COMSOL 3.5 Multidisciplinary software. An automated mesh with typically 50,000 degrees of freedom was generated. The first 100 or so vibrational modes of the freely supported instrument could be computed in a few tens of seconds on a desk-top PC, though many such computations were required to achieve the resolution required to identify the influence of coupling on the veering and splitting of individual modes, particular in regions of mode crossing.

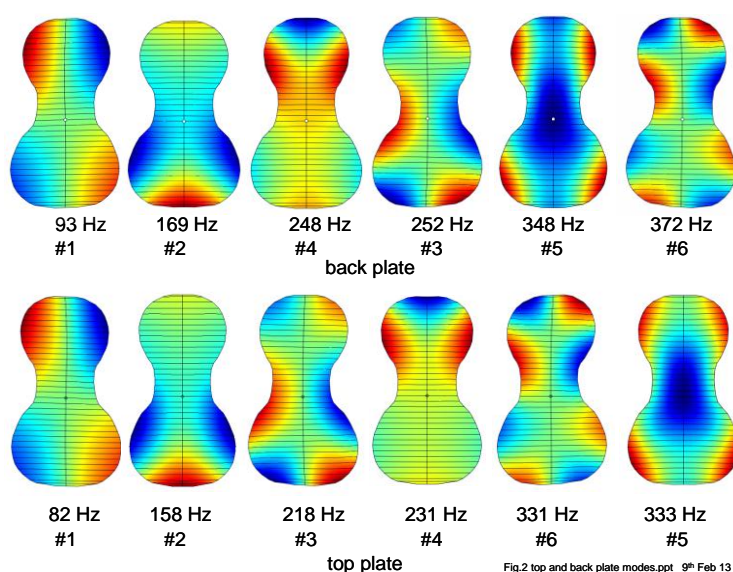
The influence on the vibrational modes of the individual plates, the ribs, f -holes, the Helmholtz f -hole resonance, a central and offset soundpost will now be considered in turn. Space precludes a

description of the computed influence of the neck/fingerboard assembly, anisotropy, and coupling to all other vibrational modes of the instrument (fingerboard, higher order cavity air modes, the tailpiece, bridge and stretched string) or the predicted radiation of sound, all of which will be described in subsequent papers. In addition, to limit the scope of this paper, only modes below 1 kHz will be considered in any detail.

3 FREE PLATE MODES

Figure 2 illustrates the computed modes shapes and frequencies of the free plates used to model the assembled instruments, before *f*-holes have been cut or bass bar added. Throughout this paper a colour scale will be used to illustrate displacements perpendicular to the plates, with dark red and blue representing equal but opposite displacements perpendicular to the plate, with the nodes at the transition between green and yellow (see figure 3).

Figure 2. The first six modes of the isotropic, uniform thickness, arched, top and back plates without f-holes.



The arching results in a strong coupling between flexural waves perpendicular to and longitudinal waves parallel to the shell surface. This can double the frequency of the low frequency plate modes, though arching becomes less important as the mode frequencies increase. Such coupling also induces significant in-plane edge contractions and extensions, which is responsible for the coupling between the bending and breathing modes of the assembled instrument. The plate frequencies will therefore be strongly dependent on how they are supported by the ribs - both in-plane and perpendicular to their edges. Figure 1 demonstrates that even relatively small changes in arching profile along the lengths of the top and back plate can reverse the order of the free-plate mode frequencies, even though their arching heights are the same.

The individual modes are either symmetric or anti-symmetric about the longitudinal central axis. This remains true for their coupled motions in the assembled instrument, in the absence of the symmetry-breaking bass bar and offset soundpost.

Mode #1 is a torsional mode of relatively little acoustic importance. Modes # 2 and #4 involve flexural bending vibrations of the lower and upper bouts respectively. Mode #2 is often referred to as the X-mode, on account of the shape of its nodal lines, though in reality they never cross. As demonstrated in the next section, the ribs couple the two modes together to form the anticlastic (curvatures in opposite directions along and across the instrument) bending mode components of the *B1-* and *B1+* signature modes.

Mode #3 is a higher order torsional mode, which includes some bending. When coupled by the ribs, these modes form the *CBR signature* mode, which is usually a relatively weak radiator of sound, though it can be excited quite strongly by an asymmetrically rocking bridge, when an offset soundpost is introduced.

Acoustically, mode #5 is by far the most important free plate mode. We will show that rib coupling transforms this mode into the volume-changing, breathing mode component of the *B1-* and *B1+* signature modes. The component breathing mode is directly or indirectly (by excitation of the Helmholtz *f*-hole resonance) responsible for virtually all the sound radiated by the violin and other stringed instruments at frequencies over their first two octaves.

4 RIB COUPLING

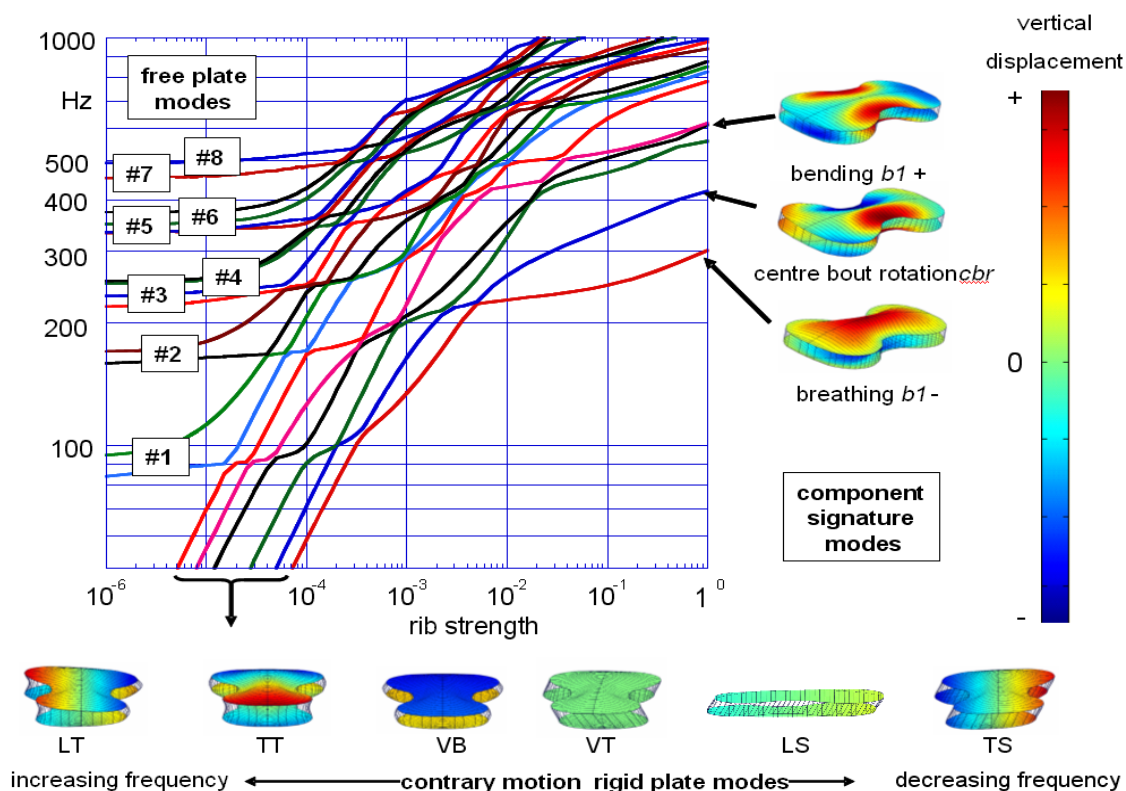


Figure 3. The computed transformation of the first eight modes of the free plates to those of the fully assembled but empty (and without *f*-holes), doubly-arched, guitar-shaped, shell structure, as a function of rib coupling strength increased from a very small value to that of a typical violin (see text). The mode frequencies are also strongly perturbed by the illustrated contrary rotational and linear displacements modes of the rigid plates about their three orthogonal axis, with unperturbed vibrational frequencies proportional to $(\text{rib strength}/\text{plate mass})^{1/2}$.

Figure 3 illustrates how the modes of the free plates are transformed into those of the assembled instrument on increasing the rib coupling “strength” from close to zero to a representative normal value. The rib coupling strength is proportional to $E_{\text{rib}}(t/h)^3$, where E_{rib} is the effective elastic constant across the ribs of height h and thickness t . In the computations, the rib height (3 cm) and thickness (1 mm) were held constant, while E_{rib} was scaled from a very small value to 10 GPa. For the cello, with its significantly larger rib height to thickness ratio, the rib coupling strength will be significantly weaker than that of the violin. This will result in relatively larger stretching and bending of the ribs.

The density was also simultaneously scaled by the same factor to maintain the frequency of the flexural rib modes at their normal high frequency, typically ~5-10 kHz for the violin and > 800 Hz for the cello (Stoppani, private communication) - well above the range of frequencies considered here. At lower frequencies, the ribs simply act as a series of parallel cantilevered springs inhibiting plate separation and bending around their edges. Nevertheless the isolated rib garland can easily be bent and twisted about its length with very little energy. Such vibrations are involved in the *CBR* and *B1*- and *B1+* signature modes of the violin, with large amplitude twisting and bending of the ribs along their edges, but relatively small amounts of stretching and bending between opposing plate edges.

Figure 3 shows that the ribs have a major influence on the frequencies and shapes of the low-lying modes of the assembled shell, which are ultimately responsible for the signature modes of the fully modeled instrument. The coupling is especially strong between free plate modes with matching mode shapes and closely spaced frequencies.

As well as the coupled free plate modes, there are six additional modes involved in the coupled plate vibrations. These are derived from the twelve zero-frequency degrees of freedom of the two isolated plates, which describe their rigid body displacements along and rotations about their three orthogonal symmetry axis. Six of these simply become the rigid whole-body linear displacements and rotations of the assembled instrument.

The remaining six modes are transformed into modes with linear displacements and rotations of the rigid plates in opposite directions, as illustrated in Figure 3. Because such vibrations involve the stretching and compression of the ribs, their frequency will increase with rib strength as $\sqrt{E_{\text{ribs}}/M_{\text{plates}}}$, where M_{plates} will be a mode-specific effective plate mass. Their unperturbed frequencies therefore increase with slope $\frac{1}{2}$, when frequency and rib strength are plotted in figure 3 on logarithmic scales.

At intermediate coupling strengths, these modes cross and couple to any of the flexural wave modes of the top and back plates sharing a common symmetry. This results in considerable veering and splitting of several mode frequencies in the cross-over region. The splitting of modes is proportional to the rib-induced interaction strength. Modes not sharing a common symmetry do not interact. Their frequencies simply cross.

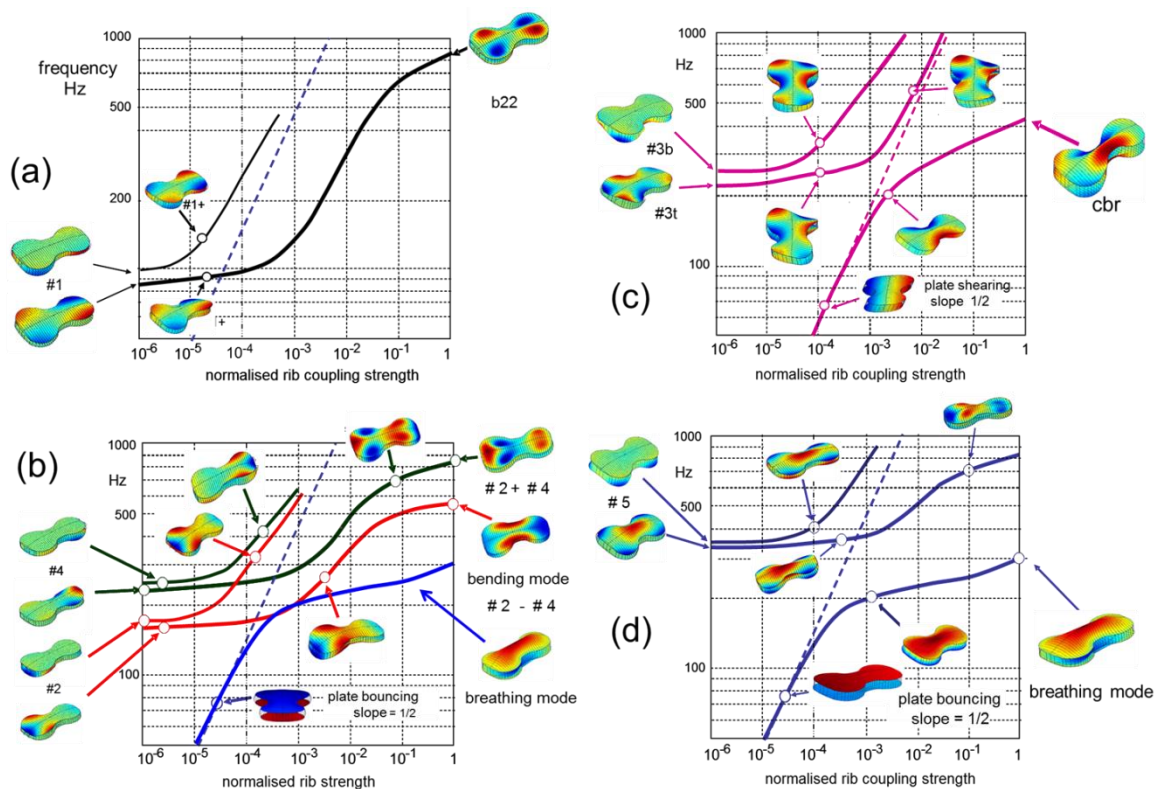
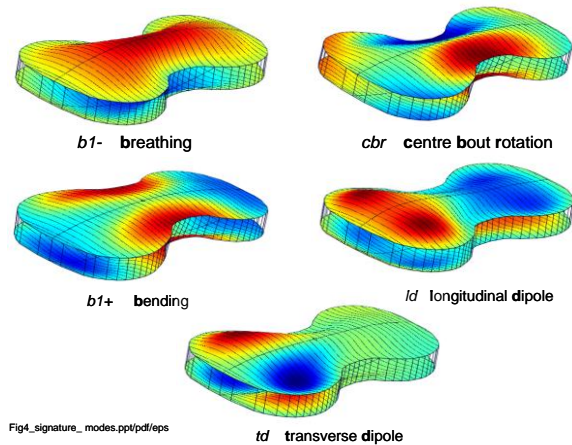
At full coupling strength, the influence of the rigid plate modes are less important, but still account for the small amounts of rib stretching, bending, rotation and twisting observed in experimental modal analysis measurements. Because of these interactions, the dependence of shell mode frequencies on rib strength is rather complicated and frequently difficult to interpret. Therefore, in figures 5a-d below, we have extracted those parts of the dispersion curves that identify the transformation of specific plate modes into the low frequency modes of the assembled instrument.

Before leaving figure 3, it is important to note that, despite the complexity of the modal frequency plot, the number of modes of the assembled structure is always conserved and is equal to the number of initial modes of vibration involved. It is therefore possible to follow every single mode of the interacting system from those of the uncoupled plates to the modes of the fully coupled structure, as the modes are adiabatically (smoothly) transformed on increasing the rib coupling strength over many orders of magnitude. However, as the coupling strength increases each mode increasingly includes additional coupled component vibrations of the initial system. As a result of the increase in

mode frequencies with increasing rib strength, the number of low frequency modes of the shell at full coupling strength is relatively small.

The five lowest modes of the assembled shell are illustrated in Figure 4. These will be referred to as the *cbr* (centre bout rotation), *b1-* (breathing), *b1+* (bending), *ld* (longitudinal dipole) and *td* (transverse dipole) modes of the empty shell. Note the use of small letters to denote what eventually become contributing component vibrational modes of the non-interacting *CBR*, *B1-* and *B1+* normal modes of the assembled instrument.

Figure 4. The first five component or basis modes of the assembled guitar-shaped box at full rib-coupling strength.



Figures 5a-d. Extracted dispersion curves for the transformations of the first five free plate modes to the lowest frequency modes of the assembled shell.

The transformation of each of the first five free plate modes into the modes of the freely supported assembled shell will now be described.

Figure 5a illustrates the influence of rib coupling on the #1 torsional plate mode. At even very small coupling, the top and back plates are coupled together to form two new modes with the plates twisting in either the same or opposite directions. Twisting in the same direction avoids stretching the ribs. This mode therefore increases far less rapidly with rib coupling strength than the higher frequency mode, which rapidly rises in frequency into the multiplicity of flexural plate modes above 1 kHz. In contrast, the frequency of the mode with plates twisting in the same direction increases more slowly with rib strength to become a *transitional* mode between the low frequency *signature* modes and the closely spaced, overlapping (because of damping) higher frequency modes of the assembled shell.

Figure 5b illustrates a similar initial behavior of the free plate modes #2 and #4, with the component pair of coupled lower and upper bout bending vibrations in opposite directions again increasing very rapidly in frequency because of the stretching of the ribs. The stretching of the ribs of all coupled symmetric plate modes vibrating in opposite directions involves a strong interaction with the rising frequency (slope $\frac{1}{2}$) bouncing mode. Such modes therefore all contribute to the strong veering of the bouncing mode, which transforms smoothly into the *breathing* mode of the assembled shell.

In contrast, the coupled #2 and #4 plate modes bending in the same sense simply cross the rising *bouncing* mode frequency. The lower of these pair of modes transforms into the *b1+ bending* mode of the assembled shell, with the longitudinal bending of the original #2 and #4 modes flexing in both bouts and both plates in the same directions. This involves large plate edge displacements made possible by the ease with which the rib garland can be bent in this way. The upper mode retains the original symmetry of the lower bout bending of the individual plates, but is now coupled to a *breathing* mode in the upper bout, with both component sets of vibration confined within the plate edges. This mode may well be responsible for the strong peak in monopole radiation observed by Curtin¹¹ for a couple of Stradivari violins at around 1 kHz.

As illustrated in figure 5c, the modal frequency of the coupled anti-symmetric free plate #3 modes vibrating in opposite senses, behaves in much the same way. The mode increasing rapidly in frequency, as it interacts strongly with the rapidly rising frequency of the lengthwise axial rotations in opposite directions of the rigid plates. In contrast, the mode with the plate vibrating in the same sense now interacts strongly with the rigid plate transverse shearing mode. After crossing this mode, the emerging *cbr* mode still retains the centre bout rotation, but acquires an additional shearing component. The shearing component leads to a rhombohedral distortional vibration of the central bout cross section, which explains the origin of the *CBR* name - Centre Bout Rhombohedral displacements. However, we prefer the name Centre Bout Rotation, as it is its rotation rather than shear motion that determines how strongly it is excited by the string-induced rocking of the bridge. The *cbr* mode involves little change in volume, so it usually plays relatively minor role in the acoustics of the violin.

Figure 5d again illustrates a strong interaction of the pair of #5 plate modes vibrating in opposite senses with the rapidly rising frequency, rigid plate, bouncing mode. This leads to the rapid increase in frequency of this mode with increasing rib coupling strength and a strong contribution to the veering of the bouncing rigid plate mode, which transforms into the *b1- breathing* mode. In contrast, the mode initially describing the coupled #5 vibrations of the two plates vibrating in the same direction, is unaffected by any of the contrary-motion rigid plate modes. It therefore increases monotonically with increasing rib strength, to become one of a number of relatively unimportant modes in the transitional frequency regime. In summary:

- the combination of #3 free plate modes vibrating in the sense are transformed into the *cbr centre bout rotation* mode of the assembled shell.
- the combination of #2 and #4 plate modes vibrating in the same sense in the upper and lower bouts of both the top and back plates transforms into the *b1+ bending* mode.

- the combination of #2, #4 and #5 shell modes vibrating in opposite senses in the top and back plates transform the rigid plate bouncing mode into the *b1- breathing* mode. This mode is largely responsible for all the radiated sound in the monopole signature mode regime at low frequencies, as it is the only mode with a significant volume change.

For all modes, the frequencies are still weakly rising at full rib coupling strength. This reflects the transition from pinned to clamped boundary conditions at the plate edges.

5 ISLAND AREA

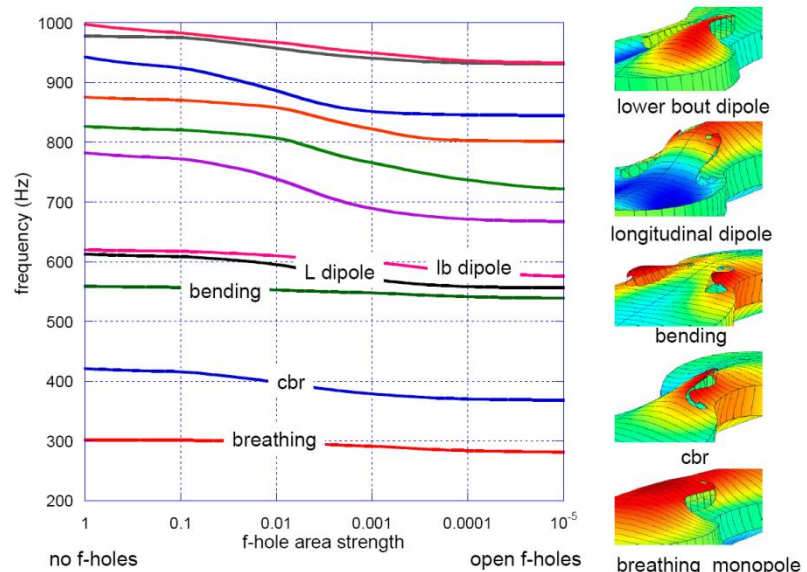
The open *f*-holes on the front plate and the island area between them play a major role in the sound of the violin and related instruments, as recognized by Cremer¹ (chpt.10). Firstly, the open holes in the front plate introduce the *A0* Helmholtz cavity resonance, which boosts the sound of all members of the violin family over their first octave or so. Secondly, the free *f*-hole edges define the shape of the island area, which strongly influences the penetration of flexural waves from the lower and outer bouts towards the two feet of the rocking bridge, which excite them. Thirdly, the island area does not have to bend as much as the outer plate edges attached to the ribs. This results in an increased change of volume of the shell as it bends. This contributes to the coupling between the bending and breathing vibrations, which is such an important feature of the signature modes of the assembled instrument. As described later in this paper, the penetration of flexural waves into the island area and resulting excitation of radiating modes is also strongly influenced by the strength and position of the soundpost in the island area – and by offset bass bar and extra loading of the bridge and strings.

6.1 The island area

Figure 6 illustrates the influence of the *f*-holes on the low frequency flexural wave modes of the shell. The frequencies were computed as a function of *f*-hole strength varied by simultaneously decreasing the elastic constant and density of the *f*-hole areas by the same factor from unity (no *f*-holes) to 10^{-5} (effectively open *f*-holes).

Figure 6. The influence of the *f*-holes on the empty shell mode frequencies and shapes in the island area.

Opening the *f*-holes has little effect on mode shapes, but lowers their frequencies by increasing their penetration into the island area towards the free edges of the island area. As a result, the inside edges of the *f*-holes can vibrate with larger amplitudes, almost independently from the outer edges constrained by the ribs, as illustrated.



6.2 The Helmholtz *A0* resonance.

The combined open area *A* of the two *f*-holes together with the volume *V* of the internal cavity, if rigid, would form a Helmholtz resonator, with resonant frequency

$$2\pi f_{Helmholtz} = c_o \sqrt{gA^{1/2}/V}, \quad (1)$$

where c_o is the velocity of sound within the cavity and g is a f -hole shape-dependent constant of order unity.

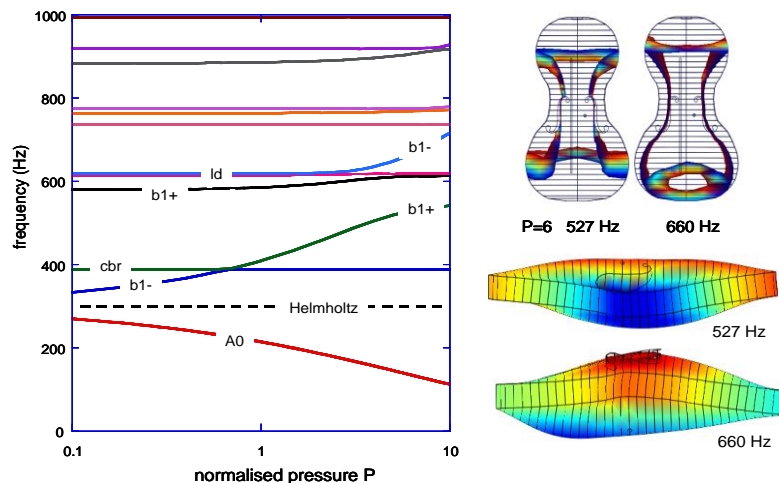


Figure 7. The variation of the low frequency modes of the empty guitar-shaped shell with f -holes cut into the top plate, as a function of ambient pressure normalized to normal air pressure. The dashed line indicates the unperturbed Helmholtz frequency of 307 Hz. Also illustrated are the mode shapes and reversed *baseball-like* nodal lines of the coupled $b1$ -breathing and $b1+$ component bending modes.

Although the Helmholtz frequency, proportional to the velocity of sound in air, is independent of pressure, the strength of the coupling between the induced cavity pressure fluctuations and flexural plate vibrations that excite them is proportional to the ambient pressure. Figure 7 illustrates the dependence of the shell modes and $A0$ f -hole frequencies on ambient pressure.

The computations make the usual simplifying assumption that the pressure within the cavity is uniform. The pressure results from the volume changes of the modes exciting the Helmholtz resonance, which also reacts back on the shell wall vibrations themselves. Therefore, only those modes with a significant volume changing component are affected by their coupling to the Helmholtz resonance. Such modes will also radiate strongly in the signature monopole regime. For the empty shell, these are the $b1$ -breathing and, to a lesser extent, the $b1+$ bending modes.

The computations confirm the very strong perturbation of the $A0$ and $b1$ -breathing modes, as the ambient pressure is increased. At zero pressure, implicitly assumed in the previously described computations, the computed empty shell breathing mode frequency of around 300 Hz is very close to that of the ideal Helmholtz resonator at 309 Hz. On increasing the internal pressure to a “normal” ambient value, the coupling is so great that the predicted $A0$ mode would drop to around 200 Hz, while the breathing mode would be raised to around 400 Hz. Analytic models predict that the product of the resulting $A0$ and $b1$ -mode frequencies should remain constant, as confirmed by the computations.

In practice, computations show that the internal pressure driving the Helmholtz vibrations of the air in and out of the f -holes is reduced below the average pressure, because of significant pressure drops associated with the flow of air from the upper and lower bouts. This reduces the effective pressure driving the f -hole resonance by a factor of ~ 0.7 , which is equivalent to reducing the effective ambient pressure by the same factor. Measurements on violins with and without soundposts by Stoppani (private communication) show typical drops in the $A0$ frequency from around 280 Hz to 240 Hz, in qualitative agreement with the above model.

Initially, none of the other modes are significantly affected by changes in ambient pressure. However, as the pressure increases, the frequency of the $b1$ -breathing mode approaches and would otherwise cross that of the $b1+$ bending mode. Because both modes share similar in-plane contractions and extensions around the edges of the plates they are relatively strongly coupled. They then form what become the $B1$ - and $B1+$ modes of the assembled instrument with bending

and breathing component vibrations in either the same or opposite phases, as illustrated in figure 7. Their combination also demonstrates the illustrated reversal of the baseball like nodal lines of the two modes, which is one of the characteristic features of such modes in real instruments. In addition there is a somewhat smaller interaction with the higher frequency longitudinal dipole mode illustrated in figure 4 and a higher frequency mode just above 900 Hz. Moreover, the $b1-$ and $b1+$ modes never cross, but become the in and out of phase vibrational components of the $B1-$ and $B1+$ normal modes of the assembled instrument.

6. THE SOUNDPOST

Below 10 kHz or so, the soundpost acts as a fairly rigid beam exerting equal and opposite forces and couples to the plates across its ends. This imposes almost equal displacements and slopes of the plates across its ends assuming intimate contact with the plates. This adds a localized, flexural wave mode to the modes of the open shell structure, with a singularity at the origin for an applied point force and decaying exponentially as $e^{-kr}/r^{1/2}$ at large distances. The wave vector $k=2\pi/\lambda$ is given by the usual flexural wave dispersion relationship, $\omega \sim tk^2$, determining the wavelengths λ of the standing waves in the upper and lower bouts (t is the plate thickness). The soundpost locally perturbs the modes of the empty shell to give almost equal displacements across its ends. However, they need not be at exact nodes, as the two ends can still vibrate in the same direction.

When located within the island area, the soundpost acts as a gate inhibiting the penetration of flexural waves in the lower bout past the soundpost into the upper bout and vice versa, as illustrated in figure 7. The flexural wave amplitudes close to the soundpost are rather small and vary rapidly with distance. The soundpost's position relative to the two feet of the bridge exciting the mode vibrations is therefore crucial in terms of the strength with which modes are excited and hence the intensity and perceived quality of the radiated sound. This is why the soundpost position is so critical in setting up a violin for optimal sound quality.

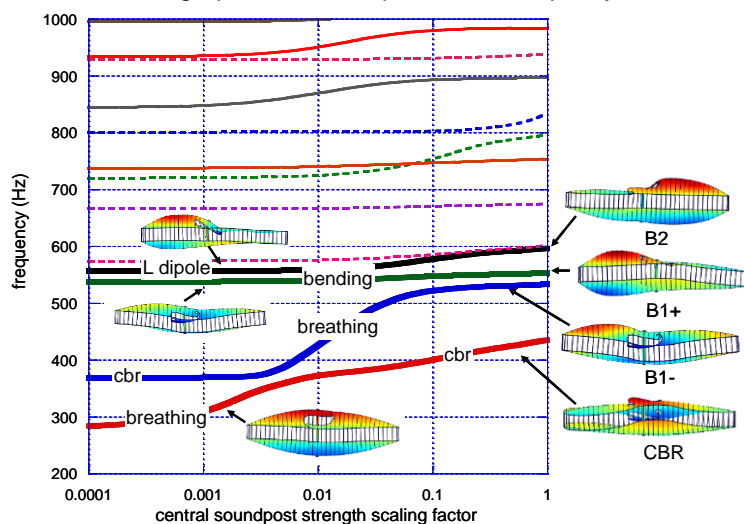


Figure 7. Influence on mode frequencies and shapes of the strength of a centrally placed soundpost. The thin dashed lines represent anti-symmetric shell modes and solid lines symmetric modes.

The dependence of mode frequencies on the strength of a centrally placed soundpost in-line with the f -hole notches is illustrated in figure 7 for the shell without bass bar and finger-board/neck, neglecting coupling to the Helmholtz cavity resonance.

The soundpost strength is varied by simultaneously increasing its elastic constant and density by the same factor to maintain its resonant modes at typical value above ~ 5 kHz for the violin. A central soundpost can only strongly perturb the symmetric shell modes.

The most important feature is the strong increase in frequency of the $b1-$ breathing mode. This first crosses the frequency of the cbr mode with a small amount of coupling-induced veering and splitting of mode frequencies. The frequency then continues to rise, approaching and otherwise crossing the initially higher frequency $b1+$ bending mode. In the crossover region, all three nearby $b1-$ breathing, $b1+$ bending, and longitudinal dipole ld component vibrational modes are coupled together to give three new $B1-$, $B1+$ and $B2$, non-interacting, normal modes of the shell. The sound

radiated by each mode will be determined by the strength of its coupled $b1$ -breathing component and the strength with which it is excited by the rocking bridge.

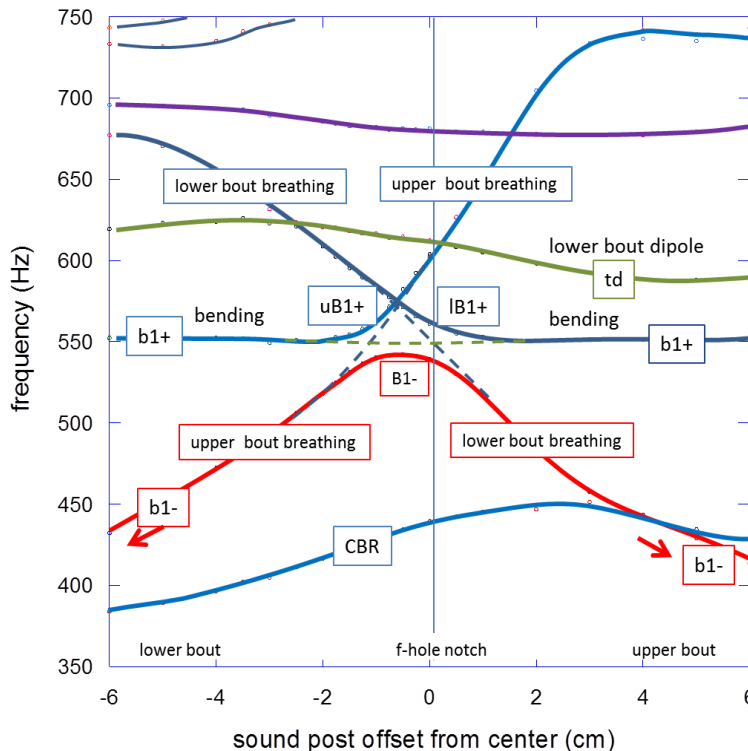


Figure 8. Influence on mode frequencies of shifting the soundpost along the central axis

As the soundpost is moved along the central axis towards the lower bouts, the decrease in frequency of the higher frequency upper bout $ub1$ -mode and increase in frequency of the lower bout $lb1$ -mode result in the modes crossing. In our model, their frequencies would coincide for the soundpost about 1 cm behind the bridge. As evident from figure 8 these two modes are effectively orthogonal as they cross without any evident mode veering or splitting. However, both breathing modes are relatively

strongly coupled to the $b1+$ bending mode, leading to the veering and splitting of the modes on either side of coincidence. This results in the maximum in the frequency of the lower mode, which changes in character from a breathing mode largely localized within the lower bouts to an equivalent mode largely localized in the upper bouts as the sound post is moved across the maximum towards the lower bouts.

The low frequency mode at coincidence involves breathing modes of similar amplitudes in both the upper and lower bouts. This mode is similar to the $b1$ -breathing mode of the empty shell with a soundpost induced minimum near the centre of the violin. In contrast, the two degenerate higher frequency modes involve breathing mode components of opposite polarities in the upper and lower bouts, with relative amplitudes that change on moving away from coincidence. This mode is very similar to that of the ld longitudinal dipole mode of the empty shell, with its node near the soundpost position. The relationship of the above modes to those of the empty shell suggests the value of measuring the vibrational modes of the empty shell as a characterization tool (Stoppani⁵), especially since such measurements can easily be made before the final thickness graduation of the plates.

The influence of offsetting the centrally placed sound post away from the central axis is illustrated in figure 9. The frequencies of both $lB1$ - and $uB1$ -breathing modes are decreased as the soundpost, acting rather like a gate, is moved sideways. This opens up the pathway through the island area on the bass side allowing the lower and upper bout breathing vibrations to penetrate further into the opposite bout, hence lowering their frequencies. This results in a twisting of the central bout region pivoting about the soundpost position. Just as for lengthwise offsets of the soundpost, the most important effect of sideways offsetting is to modify the coupling of the modes to the now asymmetrically rocking bridge. The asymmetry introduced by the offset soundpost (and to a lesser extent the bass bar) allows the horizontal component of the bowed string force to excite the symmetrical breathing modes and hence radiate sound, even though the frequency of the higher frequency modes is scarcely affected by offsetting the soundpost.

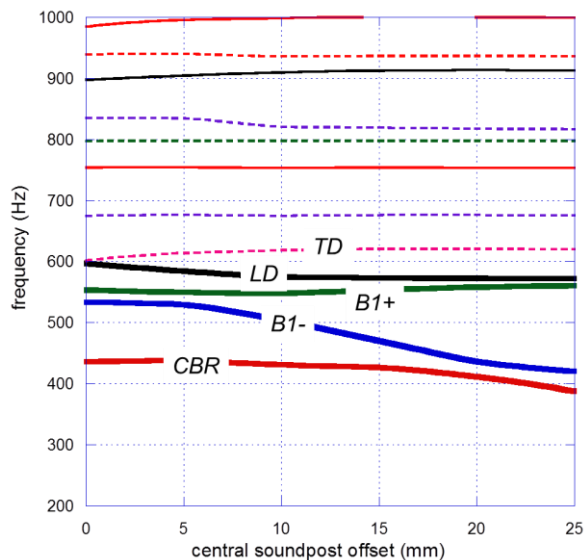


Figure 9. The influence of offsetting a centrally placed sound post from the central axis.

The added influence of anisotropy, bass bar, fingerboard-neck assembly and coupled air modes and the interaction of the shell modes with the vibrational modes of higher order air modes, the fingerboard, the bridge and bowed strings, and the resulting radiation of sound will be described elsewhere. However, because the mode shapes described in this paper are largely determined by the symmetry of the guitar-shaped shell, they will be common to all instruments of the violin family, even if their relative frequencies and excitation strengths may vary from one instrument to another within the same class and certainly between the violin, viola, cello and basses

7. HIGHER FREQUENCY MODES

Space precludes any detailed discussion of the computed higher frequency modes between 1 and 4 kHz. However, because it is only possible to localise an integral number of half-wavelength in the upper or lower bouts of the top or back plates at specific frequencies, the modes of the assembled shell become increasingly localized in one of the four locations. Specific localised modes always first appear in the lower bout of the more flexible top plate. The localised modes with common symmetries and frequencies are weakly coupled via the central bout regions giving composite modes with generally very different vibrational amplitudes in each of the four weakly coupled surface areas, as described in a subsequent publication.

8. REFERENCES

- [1] L. Cremer, *The Physics of the Violin*, MIT, Chapter 10 (1984).
- [2] C.R. Calladine, *Theory of shell structures*, Cambridge Univ. Press (1983).
- [3] K.D. Marshall, 'Modal analysis of a violin', *J. Acoust. Soc. Am.*, vol. 77, no.2, 695-709 (1985).
- [4] G. Bissinger, 'Structural acoustics of good and bad violins', *J. Acoust. Soc. Am.*, Vol. 124, No.3, 1764-1773 (2008).
- [5] G. Stoppani, to be published in *Proc. SMAC2013*, KTH, Stockholm.
- [6] G.A. Knott, A modal analysis of the violin, MSc Thesis, Naval Postgrad. School, Monterey, pp 507-550, in *Research Papers in Violin Acoustics 1975-1993* (ed. C.M Hutchins and V. Benade), *Acoust. Soc. Am.* (1997).
- [7] G.W. Roberts, Finite element analysis of the violin (PhD Thesis, Cardiff,), pp. 575-590 in *Research Papers in Violin Acoustic 1975-1993* (ed. C.M Hutchins and V.Benade), *Acoust. Soc. Am.* (1997).
- [8] J. Bretos, C. Santamaria and J.A. Moral, 'Vibration patterns and frequency responses of the free plates and box of a violin obtained by finite element analysis', *Jnl. Acoust. Soc. Am.*, vol. 105, no.3, 1942-1950 (1999).
- [9] O.E. Rodgers and P. Anderson, 'Finite Element Analysis of a Violin Corpus', *Catgut Acoust. Soc. Jnl*, No.4 (Series II), 13-26 (2001).
- [10] S. Zygmuntowicz, 'The Titian Strad', *The Strad*, February, 30-34 (2009).
- [11] J. Curtin, 'Measuring violin sound radiation using an impact hammer', *J. Violin Soc. Am.*, VSA Papers, Vol 22, no. 1, 186-208 (2009).